Available online at www.sciencedirect.com

ScienceDirect

Ceramics International 40 (2014) 1263–1272

CERAMICS INTERNATIONAL

www.elsevier.com/locate/ceramint

Short communication

Evaluation of residual stress in microplasma sprayed hydroxyapatite coating by nanoindentation

Arjun Dey[a,*], Anoop K. Mukhopadhyay[b]

[a]*Thermal Systems Group, ISRO Satellite Centre, Indian Space Research Organisation, Vimanapura Post, Bangalore-560017, India*
[b]*CSIR—Central Glass and Ceramic Research Institute, Kolkata-700 032, India*

Received 14 January 2013; received in revised form 25 May 2013; accepted 19 June 2013
Available online 27 June 2013

Abstract

The evaluation of residual stress in bioactive hydroxyapatite (HAP) ceramic coating by nanoindentation technique has been attempted successfully for the very first time ever in the present work. The HAP coatings were deposited on surgical grade 316 L austenitic stainless steel and Ti–6Al–4V substrates by microplasma spraying (MIPS) process. The coatings had Ca/P ratio of 1.67 and were ~80–90% crystalline. The results showed a residual compressive stress of ~22 MPa for the MIPS-HAP coatings on the SS316L substrates. For the coatings deposited on the Ti–6Al–4V substrates, however, a residual tensile stress of ~11 MPa was estimated. These data matched well with those obtained by XRD based technique. Thus, favorable data comparison provides further support to the efficacy of the nanoindentation based technique utilized in the present work for residual stress estimations.

Keywords: Hydroxyapatite; Coating; Microplasma spraying; Residual stress; Nanoindentation

1. Introduction

The bioactive hydroxyapatite (HAP) coatings on metallic substrates are well known for prosthetic applications. Many deposition techniques like sputtering, electrophoretic deposition, sol–gel techniques, biomimetics, electrohydrodynamic atomization spraying, dip/slurry coatings as well as plasma spraying etc. have been utilized by the researchers to deposit HAP coatings. However, as of now globally the plasma spraying process is the only commercially accepted method for development of the HAP coatings for in vivo applications.

The deposition of the HAP coatings by the microplasma spraying process (MIPS) is a better and greener process [1–7]. This technique utilizes a lower plasmatron power (~1.5 kW). Thus, the power requirement and the energy intensiveness of the MIPS process is much lower than that (10–40 kW) required by the conventional macroplasma spraying process (MAPS) [8–19]. It has been already demonstrated by the present author and coworkers that the MIPS-HAP coatings on stainless steel (SS316L) substrates possessed a high degree of crystallinity and porosity without major degradation of mechanical properties e.g. bonding strength, micro/nano-hardness, fracture toughness, scratch resistance and Young's modulus [1–6]. In vivo experiments also confirmed the very promising features of osteointegration for the MIPS-HAP coated implants e.g., intra-medullary pins [7].

However, it is already well known that the quenching induced and thermal mismatch induced stresses are the two main contributors to the overall residual stress in plasma sprayed coatings [8]. The in-service reliability of such bioactive HAP ceramic coated implants is determined by their long term performance. In other words the performance can be very adversely affected due to the unwanted yet unavoidable presence of residual stress inside the coating or at the coating-substrate interface. If the residual stresses are high enough it may more often than not lead to cracking and/or buckling of the coating. Such a situation is not at all desirable for a HAP coated bio-implant. Therefore, it is essential to study the nature and extent of residual stress condition in the coating.

It is, therefore, very important to note in this context that in general the crystallinity of the MIPS coatings is much higher

*Corresponding author. Tel.: +91 80 2508 3214; fax: +91 80 2508 3203.
E-mail addresses: arjundey@isac.gov.in, arjun_dey@rediffmail.com (A. Dey).

0272-8842/$ - see front matter © 2013 Elsevier Ltd and Techna Group S.r.l. All rights reserved.
http://dx.doi.org/10.1016/j.ceramint.2013.06.073

than those of the MAPS coatings [2,4]. It happens due to the fact that lesser power inputs of the MIPS process itself translate to reduction of overheating of the molten splats that often leads to amorphous phase formation in the MAPS-HAP coatings. This reduction in amorphous phase formation most likely can cause a corresponding enhancement in the overall degree of crystallization available in such a microstructure. This enhancement in crystalline nature of the microstructure would certainly help to reduce the residual stress in such coatings simply because the more properly the crystals are grown the quicker the misfit strains shall diminish. Moreover, it is already well established that the porosity level of MIPS coatings is much higher than those of the MAPS coatings [1–6]. These microstructural porosities may further act as a cushion to accommodate the misfit strains and there by, do definitely raise a possibility to reduce the residual stress.

A typical collation of literature [9–19] on residual stress data of HAP and HAP composite coatings is presented in Table 1. These data indicate that the numerical magnitude of residual stress may vary over at least two orders of magnitude e.g., from as low as ~5 MPa to as high as ~450 MPa. These data also strongly highlight the fact that there has not been any report yet on the magnitude and nature of the residual stress state in MIPS-HAP coatings by the nanoindentation technique. It also emerges from this survey (Table 1) that a comparative assessment of the residual stress magnitude and nature evaluated by the nanoindentation technique in MIPS and MAPS-HAP coatings has not yet been explored as well.

Several researchers [9–11,13,15,19] reported the state of residual stress in HAP or HAP composite coatings on Ti–6Al–4V or Ti substrate as to be tensile in nature. However, others [11,12,14,16–18] have estimated the residual stress states of the HAP coatings on similar substrates as to be compressive in nature. Thus, it is clear from the literature data that the nature of the residual stress state in HAP coatings is yet to be unequivocally established.

There is also the presence of a significant problem in the literature data [9–19]. The problem is that since there does not exist any unique standard prescribed method for evaluation of residual stress in HAP coatings, it is nearly impossible to compare one reported data with another. It is also noted from the data given from Table 1 that a huge variety of methods have been utilized for the estimations of the residual stress states in the HAP coatings. For instance, the methods so far utilized for residual stress determinations in HAP coatings can typically include (a) the applications of the Hooke's law ($\sigma = E\varepsilon$), (b) the X-ray diffraction ($\mathrm{Sin}^2\psi$) technique, (c) the Raman piezo-spectroscopy, (d) the material removal techniques (e.g., the hole drilling, layer removal etc.) and (e) the mathematical modeling techniques (i.e., analytical or numerical) [9–19].

Each of the aforesaid techniques has its own advantages and disadvantages [9–19]. Therefore, the technique must be very judiciously chosen. For example, the X-ray diffraction e.g., the ($\mathrm{Sin}^2\psi$) technique can determine the residual stress only in a thin surface layer assuming that it behaves as a bulk, defect free, ideally isotropic material. However, in such cases where these assumptions do not strictly hold well, the very applicability of the ($\mathrm{Sin}^2\psi$) technique can be a debatable issue. On the other hand, when it is needed to determine the residual stresses in thick layers of either a graded or an inhomogeneous composition; the materials removal method can be the suitable method of choice. It should be appreciated that both the '$\mathrm{Sin}^2\psi$' and the materials removal techniques are non-destructive in nature. But the unique advantage of the '$\mathrm{Sin}^2\psi$' technique is that it can offer a spatial resolution much superior than that can be achieved by the material removal methods. Another unique advantage of the '$\mathrm{Sin}^2\psi$' technique is of course that it can be applied to complicated geometries while the material removal methods can be used only for simple specimen geometries.

In this quest for the suitable method for evaluation of residual stresses in thin and thick film materials as well as bulk

Table 1
Literature status on residual stress of HAP coating.

System: coating/substrate	Processing route	Method	Residual stress (MPa)	References
HAP/Ti6Al4V	Macroplasma spraying	Hooke's law+XRD ($\sigma = E\varepsilon$)	200–450	Brown et al., 1994 [9]
HAP/Ti6Al4V	High velocity oxy fuel technique	Hooke's law+XRD ($\sigma = E\varepsilon$)	70–110	Brown et al., 1994 [9]
HAP/Ti6Al4V	Macroplasma spraying	Raman piezo-spectroscopy	(−60)–100	Sergo et al., 1997 [10]
HAP/Ti	Macroplasma spraying	Analytical model	21–41	Tsui et al., 1998 [11]
HAP/Ti6Al4V	Macroplasma spraying	XRD ($\mathrm{Sin}^2\psi$)	(−5) –(−17)	Yang et al., 2000 [12]
HAP/Ti6Al4V	Macroplasma spraying	XRD ($\mathrm{Sin}^2\psi$)	88	Han et al., 2001 [13]
HAP/Ti6Al4V	Macroplasma spraying	XRD ($\mathrm{Sin}^2\psi$)	(−17)–(−27)	Yang and Chang 2001 [14]
HAP/Ti6Al4V	Macroplasma spraying (Vacuum)	Hooke's law+XRD ($\sigma = E\varepsilon$)	21	Gledhill et al., 2001 [15]
HAP/Ti6Al4V	Detonation gun sprayed	Hooke's law+XRD ($\sigma = E\varepsilon$)	29	Gledhill et al., 2001 [15]
HAP/Ti6Al4V	Macroplasma spraying	XRD ($\mathrm{Sin}^2\psi$)	(−12.5)–(−29)	Millet et al., 2002 [16]
HAP/Ti6Al4V	Macroplasma spraying	XRD ($\mathrm{Sin}^2\psi$)	(−16)–(−18)	Yang and Chang, 2003 [17]
HAP/Ti6Al4V	Macroplasma spraying	XRD ($\mathrm{Sin}^2\psi$)	(–36)–(−78)	Yang and Chang, 2005 [18]
HAP/Ti6Al4V	Macroplasma spraying	Materials removal	(−36)–(−53)	Yang and Chang, 2005 [18]
Fluoridated HAP-β−TCP/ Ti6Al4V	Sol–gel technique	XRD ($\mathrm{Sin}^2\psi$, $\psi = 90^\circ$)	79–286	Cheng et al., 2007 [19]
Fluoridated HAP-β-TCP/Ti6Al4V	Sol–gel technique	$\sigma = (\Delta\alpha x \Delta t x E)/(1-\nu)$	50	Cheng et al., 2007 [19]
HAP/SS316L	Microplasma spraying	Nanoindentation	(−22)	Present study
HAP/Ti6Al4V	Microplasma spraying	Nanoindentation	11	Present study

materials; the novel nanoindentation technique [20–24] offers several potential advantages. The first unique advantage of this method is that it is less tedious. The second unique advantage is that it is less time consuming. The third and possibly the most unique advantage of this method is that it can be utilized for the estimations of both the residual stresses and the plastic strains. The ease and convenience with which such measurements can be done as well as the accuracy with which such measurements can be made are definitely far superior to those offered by the more conventional methods. Such 'conventional methods', comprise of the techniques such as the hole drilling, layer removal, strain evaluation, displacement/curvature measurements, piezo-spectroscopy, X-ray diffraction, neutron diffraction etc. as already mentioned above.

In addition, the same nanoindentation technique as mentioned above can be utilized to extract both local and volume-averaged global properties such as Young's modulus, yield strength, strain-hardening exponent, tensile strength and nanohardness. Now, it must be realized that residual stress may be active over both short and long ranges. The most unique advantage of the nanoindentation technique is that the one single general methodology [20] can be exploited to probe both short-range and long-range residual stresses. In terms of experimentation this can be simply achieved by a variation of the contact dimension that can be tuned over a wide range through appropriate choice of the corresponding load range e.g., μN–mN.

In this connection, it is definitely worth mentioning that this nanoindentation technique [20] has been successfully employed to measure the residual stresses in the Ti–Al–N thin films [21] as well as the Cr–Al–N thin films [22]. Similarly, for both carbon thin films [23] and B–C–N thin films [24] the efficacy of this technique [20] has been tested and found to be satisfactory. However, prior to that of the present work, there has not been any attempt so far to use this novel nanoindentation technique [20] for the measurement of the residual stress in the HAP and/or HAP composite coatings [9–19].

For the HAP coatings on Ti–6Al–4V alloys, the application of Hooke's law [9] showed that the residual stress is a sensitive function of the processing history. For instance, the coatings prepared by high velocity oxy fuel (HVOF) process had tensile residual stress of magnitude much lower (e.g., 70–120 MPa) than that (200–450 MPa) of the coatings prepared by the atmospheric plasma spraying (APS) process. Again, in the case of the coatings prepared by the atmospheric plasma spraying (APS) process, the tensile residual stress was sensitive to the composition of the gas mixture (e.g. argon/nitrogen or argon/helium) used to generate the corresponding plasma arc. The data reported in [9] also appeared to support the viewpoint that the thicker the coating would be, the higher would be the magnitude of the tensile residual stress.

Further, in complete contradiction to such observations of high tensile residual stress [9], much lower magnitude of tensile residual stresses e.g., only 20 MPa were also reported [15] for MAPS-HAP coatings deposited in vacuum on Ti–6Al–4V alloys. However, for HAP coatings deposited by the detonation gun spraying technique on the Ti–6Al–4V alloys, the residual tensile stress magnitude was a little higher at e.g., 30 MPa [15].

It was very interesting to note that the relatively dense HAP coatings deposited on the Ti–6Al–4V alloy substrates showed compressive residual stresses magnitude (e.g., ~17 MPa) that is more than three times as high as that (i.e., ~5 MPa) measured for the relatively less dense HAP coatings [12]. In this particular case, the residual porosity was reported to be only ~4 vol% in the dense but it became as high as ~10 vol% in the less dense HAP coatings. The clear message that this data [12] gave is that the denser a coating would be, the higher would be the magnitude of the residual stress frozen in it.

On the other hand, the application of the XRD based $\sin^2\psi$ method gave compressive residual stresses of ~10–30 MPa in HAP coatings of different thicknesses deposited on the Ti–6Al–4V alloy substrates [16]. In sharp contrast to these data, it has been also reported [14,17] that for MAPS-HAP coatings on the similar substrates e.g., the Ti–6Al–4V alloys the compressive residual stress may be confined to only ~16–27 MPa when evaluated by the same $\sin^2\psi$ method as was used in [16].

The data reported in [14,17] would also highlight that the magnitude (e.g., 16–27 MPa) of the compressive residual stress could also be a very strongly sensitive function of the initial temperature (e.g. ~25–500 °C) as well as the rate of heat transfer. In turn, however, the rate of heat transfer was shown [14,17] to be dependent on the variations in the nature and chemical composition of the coolant media. It is needless to mention that such coolants are generally used so that the substrate does not become overheated when the molten HAP pancakes are forced by the plasma jet to impinge onto the substrate.

The Raman piezo-spectroscopy technique has been also utilized to evaluate the residual stress of the plasma spayed HAP coatings [10]. When the coatings were deposited in vacuum a residual compressive stress of only ~60 MPa was measured by this technique. Paradoxically, however, the same technique gave a residual tensile stress of ~100 MPa; when the plasma spraying of the HAP powder was done in air [10].

It is evident from this data that the residual tensile stress was nearly 1.5 times as high as that of the residual compressive stress. The major, yet simplistic inference from this data [10] is that both the magnitude and the nature of the residual stress state are very strongly sensitive functions of the atmospheres utilized during the plasma spraying of the HAP powders. It is of further interest to note that even the application of the analytical modeling technique also did predict [11] a residual tensile stress of ~20–40 MPa for the HAP coatings deposited on Ti metal substrates.

On the other hand, the hole-drilling method gave a value of residual stress as high as~90 MPa [13]. These measurements were conducted for the MAPS-HAP coatings deposited on the surgical grade Ti–6Al–4V alloys.

Similarly, very interesting results were obtained when the material removal method [18] was applied for determination of the residual stress. It was found that there was compressive residual stress of ~30–53 MPa on the top surface of the coating. The magnitude of the same increased further to e.g., ~48–78 MPa when measured in the vicinity of the coating-substrate (i.e., HAP–Ti–6Al–4V alloy) interface.

Recently, Cheng et al. [19] estimated a residual tensile stress of ~80–300 MPa for fluoridated HAP/β-TCP composite

coatings on Ti–6Al–4V alloy substrates. In this case the XRD technique was used [19]. However, when estimated on the basis of relative differences in the respective coefficients of thermal expansions of the coating and the substrate; the magnitude of the residual stress was reported [19] to be as low as ~50 MPa. It would therefore appear from this data [19] that the judicious choice of the appropriate method can possibly play a very significant role in the correct evaluations of both the magnitude and the nature of the residual stress state in HAP coatings in general and MAPS-HAP coatings in particular.

As far as the choice of a given technique is concerned the issues which demand the most immediate attention are e.g., the coating type and the sample geometry. The chemical natures as well as the geometrical shapes of the substrates and the quality of the HAP powders utilized for coating development also assume very important roles in the selection of the method to be utilized for the residual stress state determinations. The other most important factor that must be taken into consideration is the pertinent knowledge about the processing conditions and the relevant parameters utilized for the coating development.

Thus, from the above discussions on pertinent reported literature [9–19], it is clearly evident that in spite of the wealth of literature; the data on the natures and magnitudes of residual stresses of the wide variety of HAP coatings were not so consistent always. Further, many contradictions were apparent in the literature data (Table 1). These apparent contradictions did not appear to be easily resolvable at all. Therefore, it is obvious that much more basic studies are needed to explore in more detail the residual stress states in the plasma sprayed HAP coatings. Further, it is absolutely proven from the literature data presented in Table 1 that there is no data reported at all on the evaluation of the magnitude and nature of the residual stress state by the nanoindentation technique applied to the MIPS-HAP coatings.

Therefore, the major objective of the present work was to measure both the magnitudes and the natures of the residual stress states frozen in the MIPS-HAP coatings deposited on both SS316L (HAPC/SS) and Ti–6Al–4V (HAPC/TA) substrates. It was also decided that the same would be evaluated by the novel nanoindentation technique as discussed above. In addition, it was also planned that the efficacy of the novel nanoindentation technique would be judged by the comparison of the data evaluated by this technique with those estimated by the conventional XRD based method.

2. Materials and methods

The sintered, granulated HAP powder (−53+64 μm) was synthesized in the laboratory. The conventional wet precipitation route [4] was used for the same. Two types of commercially available substrates were used. These were the surgical grade austenitic stainless steel (SS316L) and the surgical grade Ti–6Al–4V alloy. The SS316L and Ti–6Al–4V substrates were shaped into strips of about $(15 \times 15 \times 2)$ mm^3 and $(20 \times 20 \times 4)$ mm^3 sizes, respectively. To roughen their respective surfaces, the flat parallel ground substrate strips were blasted with 200–250 μm alumina grits. This step was followed by ultrasonic cleaning (Microclean-109, Oscar Ultrasonics, Mumbai, India). The cleanings were done sequentially with AR-grade acetone, ethanol and de-ionized water, respectively. Mechanical stylus profilometry technique was utilized to measure the surface roughness (R_a) values of the two the substrates used in the present work. A surface profilometer (Form Talysurf 120, Taylor Hobson, UK) was used for this purpose. The machine had a resolution of better than ± 0.01 μm.

Thereafter, the HAP coatings were deposited on both the SS316L and the Ti–6Al—4V alloy substrates. The microplasma spraying technique was utilized for the same purpose. The coatings were deposited at a low plasmatron power of ~1.5 kW. A commercial machine (e.g., Miller Maxstar 200 SD 2.5 kW, USA) with an external powder feeder chamber was used for this purpose. The input current was kept constant e.g., at ~40 A. A high purity Argon (Ar) gas was used as the primary gas for generation of plasma. The same high purity Ar gas was also utilized as the secondary gas that is required for shielding. The constant gas flow rate was 10 standard liter per minute (SLPM) for the primary gas. However, for the secondary gas the rate was just twice as high i.e., 20 SLPM. Nevertheless, the gas pressures for both the primary and the secondary gases were kept constant at 4 bar. As mentioned earlier, the plasma arc current was kept constant at 40 A during the entire duration of the spraying process. The machine had a copper anode arrangement. It was cooled by a cooling unit that used water as the coolant. The stand off distance (SOD) was maintained as to be in between 75 and 100 mm. The powder deposition rate was ~1.5 mg sec^{-1}. The average volume percentage of open porosity of the coatings as measured by the conventional image analysis technique, was typically in the range of e.g., 18–20%.

The phase compositions of the powder and the coatings were analyzed by X-ray diffraction (XRD) technique (Philips PW1710, The Netherlands). The data were recorded using the monochromatic $CuK_{\alpha 1}$ radiation at 55 mA and 40 KV. Following the method described in Ref. [25], the degree of crystallinity corresponding to the fraction of crystalline phase and/or phases present in the examined volume was evaluated from the XRD data.

Further, the lattice constants ‘a’ and ‘c’ were also calculated from the XRD data. A simple method given in Refs. [9,26] was used for this purpose. The microstructural characterizations of the MIPS-HAP coatings deposited on SS316L and Ti–6Al–4V substrates were carried out by the environmental scanning electron microscopy (E-SEM). A commercial machine (S-3400N, Hitachi, Japan) was utilized for this purpose. The E-SEM has the unique advantage that the sample does not need any preparation as is required in conventional SEM work. Thus, the as prepared, natural surface of the coating remains preserved; as any chance of creating artifacts by the preceding sample preparation work does not exist in this case.

2.1. Evaluation of residual stress by the nanoindentation technique

The nanoindentation experiments were carried out in a commercially available depth sensitive indentation machine (Fischerscope H100-XYp, Fischer, Switzerland) equipped with

a Berkovich tip. The machine had a depth sensing resolution of 1 nm. The resolution for force sensing was 0.2 μN.

The machine was calibrated following the DIN 50359-1 standard. This process involved the nanoindentation based independent evaluation of nanohardness (H) and Young's modulus (E) values of a standard reference glass block (BK7, Schott, Germany). The calibration required the measured nanohardness to be 4.14 GPa and the measured Young's modulus to be about 84.6 GPa for the BK7 glass. At least one 5 by 5 array of nanoindentations was done in the standard reference BK7 glass block for the calibration purpose. The calibration was repeated before each and every experiment. The reason for this was to ensure the reproducibility of the experimental results obtained in the present work. The Berkovich indenter used in the present work had a tip radius of about 150 nm. The semi-apex angle of this indenter was ~65.3°. The basic concept utilized for the evaluation of the residual stress by the nanoindentation technique is the following.

The shear presence of a residual compressive stress will oppose the penetration of the indenter into the coating. This will result in a lower residual depth of penetration in comparison to what would be obtained in a stress free coating. Similarly, the presence of a residual tensile stress will aid the penetration of the indenter into the coating. Such a situation will lead to a relatively higher residual depth of penetration in comparison to that would be obtained in a stress free coating. Thus, for the same given load the residual depth of penetration (h_0) in a stress free coating without the substrate will be higher than the residual depth of penetration (h_c) in a coating that has been deposited on a substrate and contains a residual compressive stress. Therefore, for the same given load the projected contact area (A_0) in a stress free coating without the substrate will be larger than the projected contact area (A_c) in a coating that has been deposited on a substrate and contains residual compressive stress.

Similarly, for the same given load the residual depth of penetration (h_0) in a stress free coating without the substrate will be lower than the residual depth of penetration (h_t) in a coating that has been deposited on the similar type of a given substrate as was conceptually considered just in the preceding paragraph and contains a residual tensile stress. Therefore, for the same given load as was considered in the preceding paragraph, the projected contact area in a stress free coating (A_0) without the substrate; will be smaller than the projected contact area (A_t) in a coating that has been deposited on a substrate and contains residual tensile stress.

Keeping this basic conceptual scenario as discussed above in mind, therefore, the depth controlled (maximum depth=1 μm) nanoindentation experiments were conducted in the present work for the evaluation of the residual stresses in MIPS-HAP coatings on the SS316L and Ti–6Al–4V substrates. The entire work was done following the method described by Suresh and Giannakopoulos [20].

According to Suresh and Giannakopoulos [20], the ratio of the projected contact area is related to the possible residual tensile stress present in a coating by the following Eq. (1):

$$\frac{A_t}{A_0} = \frac{h_t}{h_0} = \left(1 - \frac{\sigma_t \,\mathrm{Sin}\,\beta}{H_t}\right)^{-1} \tag{1}$$

Similarly, according to Suresh and Giannakopoulos [20], the ratio of projected area is linked to the possible residual compressive stress present in a coating by the following Eq. (2):

$$\frac{A_c}{A_0} = \frac{h_c}{h_0} = \left(1 + \frac{\sigma_c \,\mathrm{Sin}\,\beta}{H_c}\right)^{-1} \tag{2}$$

here, σ is the residual stress [tensile (t) or compressive (c)] of the coating. A is the projected area of the bonded coating with residual stress [tensile (t) or compressive (c)]. As mentioned earlier also, the term A_0 represents the projected area of the free standing coating without the substrate.

Further, the quantity 'h' stands for the final depth of penetration of the bonded coating with residual stress [tensile (t) or compressive (c)]. Similarly, h_0 is the final depth of penetration of the free standing coating without the substrate. H is nanohardness of the coating and the β is the angle complimentary to the semi-apex angle of the indenter. Therefore, it can be easily shown that $\beta = (90° - 65.3°) = 24.7°$.

For any given coating, at least 25 nanoindentation measurements were made at five different locations chosen randomly on the MIPS-HAP coatings. Thus, the residual stress data reported in the present work was an average of at least 25 individual data points. Further, the data had a typical standard deviation of ~12%.

3. Results and discussions

The average size (d_{50}) of the sinter-granulated HAP powder was~67 μm [2,4]. The Ca/P molar ratio was ~1.67. This was estimated from the ICP-AES data. The Ca/P ratio proved that the powder was stoichiometric in nature [2].

Although, the surface roughening treatments were the same for both the substrates, the initial asperity size distribution before such surface treatment and the final asperity size distribution after the surface treatment will never be same for any given substrate. As well, it will also never be the same after the surface treatment for the two different substrates used in the present work. It is important to note that this is exactly what has happened. Thus, the surface roughness values of SS316L and Ti–6Al–4V substrates were 2.64 ± 1.27 μm and 2.38 ± 1.88 μm respectively.

The XRD patterns of the in-house synthesized HAP powder, the MIPS-HAP coatings on SS316L and the MIPS-HAP coatings on the Ti–6Al–4V are shown in Fig. 1. For the sake of brevity, most of the times throughout the rest part of the present discussions these two coatings will be referred as HAPC/SS and HAPC/TA, respectively.

The plots of the XRD data (Fig. 1) showed the major presence of the peaks most characteristic of HAP. It can be seen that in terms of both intensities and positions of the peaks, there were

good matches between the data of the present work and that reported for the standard (JCPDS file no: 09-0432) material.

However, only one impurity phase was observed in the starting HAP powder. This was found to be due to the presence of crystalline calcium oxide (JCPDS file no: 04-0777). This might have had happened due to the decomposition of HAP into CaO at the time of sintering. Similar observations were also reported by other researchers [2,27–29].

Following the method described in Ref. 25 and using the experimentally obtained XRD data; the degree of crystallinity of the present HAP powder was calculated as ~91% (Table 2). On the other hand, other than the major crystalline HAP phases; only two minor peaks of crystalline α-TCP (JCPDS file no: 09-0348) and TTCP (JCPDS file no: 25-1137) were identified in the XRD patterns of the MIPS-HAP coatings on both the stainless steel (SS) and the titanium alloy (TA) substrates (Fig. 1). These observations of the present work were similar to the findings reported by other investigators [2,30].

The degree of crystallinity of HAPC/TA was calculated as ~89%, which was slightly lesser in comparison to that of the HAP powder e.g., ~91% (Table 2). However, the sample HAPC/SS showed a comparatively lower crystallinity of ~81% (Table 2). This was possibly due to the presence of other crystalline phases instead of HAP as mentioned earlier or due to the presence of some amorphous phases, which could have been formed during the plasma spraying process itself [2]. These important experimental observations as mentioned certainly merit discussions about their genesis. Actually, the current global knowledge base is that in any thermal spray based coating process be it macro plasma or be it microplasma, i.e., as has been

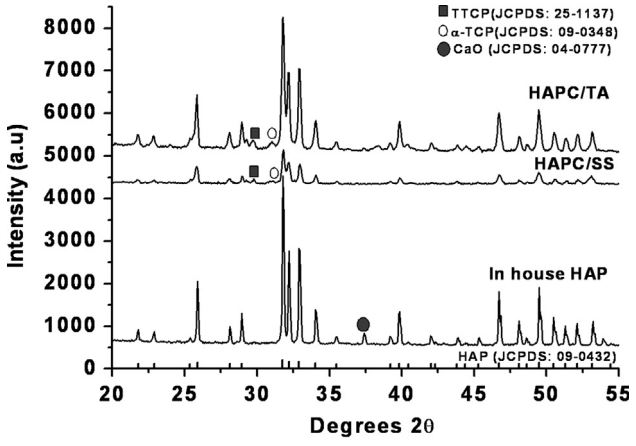

Fig. 1. XRD patterns of the in-house synthesized HAP powder and the MIPS-HAP coatings on both SS316L and Ti–6Al–4V substrates.

done in the present case, the corresponding powder e.g., the HAP powder is continuously fed from the external/internal powder feeder into the plasma jet. Typically, these powder particles are propelled at an extremely fast speed e.g., (~200 m s^{-1}) through the plasma jet and as a result they finally impinge at such ultra high velocities on the metal substrates e.g., Ti–6Al–4V alloy and SS316L [8,31].

Then what happens is the following. The molten HAP droplets capitulate and spread as splats in the shape of a pancake thereby covering a relatively larger surface area over the corresponding metal substrates e.g., Ti–6Al–4V alloy and SS316L. Almost concurrently with the event when the first molten HAP droplet arrives onto a given substrate an extremely rapid heat transfer process starts happening between the HAP coatings and the metal substrate. The exact physics of such a highly dynamic process, that will definitely have a very complex rate kinetics and the related thermodynamic states of inequilibrium; are yet to be fully understood [31–34].

Nevertheless, this process is the rate limiting step that leads to the fast solidification of the so long molten HAP pancakes over a time scale that spans over only a few μs. This is how the molten HAP pancakes will transform to HAP splats on the substrates. Therefore, it automatically follows that this rapid heat dissipation of HAP splats will have to be and it really is; directly dependent on thermal diffusivity properties of the respective metal substrates [35]. The reason for this is that, it is this particular thermal property; that primarily determines how fast or how slow the heat transport process would be allowed to occur. Thermal diffusivity of Ti–6Al–4V alloy is ~0.5×10^{-6} m^2 s^{-1}. But the thermal diffusivity of austenitic low carbon SS is almost 8 times as high (e.g., ~4×10^{-6} m^2 s^{-1}) as that of the Ti–6Al–4V alloy [36]. Thus, it is proven beyond any doubt that the heat transfer rate will be definitely much higher in the case of the MIPS-HAP coating on the SS316L substrate than in the case of the MIPS-HAP coating on the Ti–6Al–4V alloy substrate. For the same given time frame of, say 'T' units, then; the more quicker rate of heat transfer will ensure that a higher amount of heat is taken away in the case of SS316L substrate in comparison to that of Ti–6Al–4V alloy substrate. The quicker the total heat content of the molten HAP pancake is quenched out, the lesser time the structure gets for complete crystallization. So, the experimental facts as stated above would certainly suggest that the solidification process will be much more rapid in the molten HAP pancakes on the SS316L substrate than in the molten HAP pancakes on the Ti–6Al–4V alloy substrate. Due to this quicker solidification time, the complete time required for higher amount of crystallization would not be then available in the case of the SS316L substrate. On the other hand, therefore, by the

Table 2
Lattice constants and crystallinity (X_c) of the MIPS-HAP coatings.

	a=b (Å)	c (Å)	d (Å)[a]	X_c (%)
HAP powder (JCPDS no. 090432)	9.418	6.884	2.81400	100
Synthesized HAP powder	9.412	6.881	2.81151	90.51
HAPC/SS	9.404	6.896	2.81046	81.16
HAPC/TA	9.414	6.888	2.81261	89.21

[a]Lattice spacing for the (211) plane of the HAP at 100% intensity.

same logic one would expect that a relatively higher amount of time will be available for more complete or at least a relatively higher amount of crystallization in the case the molten HAP pancakes on the Ti–6Al–4V alloy substrate. This is exactly why in the present study; the MIPS-HAP coatings on the Ti–6Al–4V substrates showed a relatively higher amount of crystalline structure in comparison to those measured for the MIPS-HAP coatings on the SS316L substrates.

For the starting HAP powder the lattice constants were calculated as $a=b=9.412$ Å and $c=6.881$ Å (Table 2). However, the lattice constants of HAPC/TA were elongated (e.g. $a=b=9.414$ Å and $c=6.888$ Å in Table 2) along a $(=b)$ and c axes compared to those of the starting HAP powder.

Further, the d value (e.g., 2.81261 Å) of HAPC/TA was also slightly higher than that of the d (e.g., 2.81151 Å) value of the starting HAP powder. This data suggested the presence of a tensile residual stress in HAPC/TA. In contrast, the lattice constants of HAPC/SS (e.g., $a=b=9.404$, Table 2) along a $(=b)$ axes were slightly lower compared to those of the starting HAP powder, Table 2. Furthermore, the d value (e.g., 2.81046 Å) of the HAPC/SS sample was also slightly lower than that of the starting HAP powder. This data indicated the presence of a compressive residual stress in the HAPC/SS sample.

The experimentally measured XRD data in the present work had indeed confirmed an increase of 'd spacing', particularly those of the (211) planes, in the case of the MIPS-HAP coatings on the Ti–6Al–4V alloy substrates, and a decrease of 'd spacing' in the case of the MIPS-HAP coatings on the SS316L substrates.

In terms of the basic solid state physics drawn conceptual pictures of a solid structure; a multitude of three dimensional repetitions of the lattice plus the basis gives back the actual physical structure of a solid. The lattice structure is characterized by the 'd' values which are nothing but the spacings between the successive atomic planes. Therefore, it can be definitely argued that an increase in 'd' values may be definitely likened as a process of localized elongation at the corresponding solid's lattice structure level. This can only physically happen if the overall net stress active at that level is tensile in nature. Now, the only source of stress that could be available at that point of microstructural length scale is the residual stress.

The simple consideration of the differences in the respective coefficients of the thermal expansion coefficients of the MIPS-HAP coatings and the Ti–6Al–4V substrates would confirm that the global nature of residual stress would be tensile in nature to which all the crystals including those in the (211) planes would be exposed to. Incidentally, the case of the (211) plane has been illustrated here as a typical case in point simply because it is having the highest relative intensity e.g., 100%. It is needless to mention that this intensity is being called relative, as the intensity of the incident beam and the charge and mass of the electrons are not being considered in estimating the intensity value.

Similarly, a decrease in the 'd' values can be strongly argued to reflect a forced contraction in the corresponding solid's lattice structure level. The only agent that could be logically expected to be responsible for such contraction is the residual stress active at the solid's microstructural length scale which is directly linked to the crystalline lattices themselves present in the coating itself. As mentioned earlier, these changes in the respective 'd' values could not have had happened without any cause. In fact about a decade back it has been already proven quite conclusively by other researchers e.g., [8] that this can jolly well happen due to the overall presence of residual stress frozen in the microstructure as a result of concurrent and/or independent contributions from thermally induced stress and quenching induced stress.

However, it must be admitted also that the other XRD based method e.g., $\mathrm{Sin}^2\psi$ method is also a very potential technique to determine residual stress. But it should also be borne in mind at the same time that this particular method or for that matter any method based on XRD technique intrinsically assumes that the material under the scanner can be considered strictly as well as primarily as a crystalline bulk isotropic material.

The most burning problem that the researcher then faces in reality is that in all the cases reported in literature, the MAPS-HAP coatings can be considered neither as a typical isotropic, defect free, bulk material nor as a 100% crystalline material. This is the reality because the MAPS-HAP coatings are inherently anisotropic in structure and definitely contains microcracks, long cracks, as well as micro/macro porosity. Further, the reported crystallinity typically is not more than 50% in the MAPS-HAP coatings while it also contains other impurity phases like TCP, TTCP, CaO etc.

Hence, it is plausible to argue that it hardly matters whether it is macro and/or micro-plasma (MAPS and/or MIPS) spraying process that is used in making the coating, the structural issues remain nearly the same. Thus, the coatings deposited by any plasma spraying process will always exhibit an anisotropic microstructure that is bound to be reflected in their mechanical, thermal as well as thermomechanical behaviors and responses.

Therefore, in such a given situation as mentioned above for the heterogeneous and amorphous MAPS-HAP coatings; the bare employment as well as the realistic efficacy of any XRD based technique itself for residual stress determination is an issue that seriously remains debatable. However, even accepting the fact that the resolution of this issue is beyond the scope of the present work; it must be emphasized that this is an issue which should definitely deserve separate, dedicated attention of the research community.

Nevertheless, as reflected amply by the collation of literature data presented in Table 1, that notwithstanding these very basic issues; the XRD based methods have been used in a rather indiscriminate fashion to evaluate the residual stress values in microcracked, porous, partially crystalline HAP coatings. In fact, this basic anomaly in the whole existing literature scenario was one of the major driving forces which primarily motivated the utilization of the nanoindentation technique, for the evaluation of the residual stress in the MIPS-HAP coatings used in the present work; rather than going back again to the most commonly utilized $\mathrm{Sin}^2\psi$ method that primarily depends on the XRD technique itself.

Two representative typical micrographs of the present MIPS-HAP coatings are shown in Fig. 2 (a–b). These micrographs were obtained by the environmental scanning electron microscopy (E-SEM) technique as mentioned earlier. The complex microstructure of the present MIPS coating consisted of completely and/or partially molten, deformed and unmelted splats retaining a non-flattened core, macro- and micro-pores and inter- and intra-splat cracks. The splat size was ~50–70 μm, i.e., very similar to the average size of the original powder. The generation of unmelted splats retaining a non-flattened core was explained in detail elsewhere [2]. Generally, most of the largest particles remain almost completely unmelted because of the very low plasma power and rebound without deposition. So, most of the coating is originated by the finer fraction of the powder. Some of the finer particles may retain on the coating microstructure. The cracks occurred possibly due to the thermal expansion mismatch between those of the metallic substrate and the deposited ceramics. Further, the cracks got deflected in a random fashion in the microstructure. This was probably governed by the local thermo mechanical history that prevailed during the spraying process. Thus, all these factors as discussed above; contribute to the formation of a very heterogeneous microstructure in the present MIPS-HAP coatings. The microstructure of HAPC/SS (Fig. 2a) appeared to be denser than that of HAPC/TA (Fig. 2b).

The presence of macro and micro-porosities, and even generation of multiple cracks and their deflections have been observed for both the MIPS-HAP coatings. Generation of cracks in coatings may be thought of as to have had assisted in releasing the residual stress in the coatings. If it were really so, then; wherefrom would the further amount of residual stress come at all? Such questions may often arise and therefore it is needed to address these issues.

Further, it may be thought then that the estimation and comparison of residual stresses in the coatings with two different substrates after crack generation might create ambiguity. It is therefore very much desirable to arrive at some scenario that could help to reduce such apparently ambiguous situations as much as possible.

The residual stresses of magnitude ~21.74 MPa (compressive) and~10.75 MPa (tensile) were estimated by the nanoindentation technique for the HAPC/SS and HAPC/TA samples, respectively (Table 3). Thus, the magnitudes of the residual stresses measured in the present work were similar to the data were reported by other researchers [12,14–17].

The projected area of contact (A_0) and the corresponding nanohardness (H) of the free standing HAP coating were 8.40175×10^5 nm^2 and 4.31 GPa, respectively (Table 3). On the other hand, the HAPC/SS sample showed a projected area of contact (A_c)~8.22443×10^5 nm^2 that was slightly smaller in comparison to that (A_0) of the free standing coating, Table 3. The corresponding hardness was also slightly enhanced to ~4.96 GPa as A_c was lower than A_0, Table 3. However, the HAPC/TA sample showed a comparatively higher projected area of contact (A_t) e.g., ~8.41180×10^5 nm^2 which was slightly larger than that (A_0) of the free standing coating, Table 3. As a consequence, the corresponding hardness of the HAPC/TA sample was also slightly decreased to ~3.77 GPa, Table 3. The experimentally observed decrease of projected area of contact in the HAPC/SS sample was a signature of the presence of a residual compressive stress state in the surface. Similarly, the experimentally observed increase in the projected area of contact in the HAPC/TA sample suggested the presence of a residual tensile stress state in the surface [20]. As discussed earlier, the d value of the HAPC/SS sample was smaller than that of the starting HAP powder while that of the HAPC/TA sample was larger than that of the starting HAP powder (Table 2). These data implied that the residual stress state was compressive in the HAPC/SS sample but changed to a tensile one in the HAPC/TA sample. It is important to note that these data corroborated well with the data obtained from the present novel nanoindentation technique based evaluation of the natures and magnitudes of the residual stresses in the HAPC/SS and HAPC/TA samples.

It may be also noted further that the coefficient of thermal expansion (α) of HAP (e.g., $\alpha_{HAP}=11 \times 10^{-6}$ K^{-1} [4,12]) was much larger than the α value of SS316L (i.e., $\alpha_{SS}=18 \times 10^{-6}$ K^{-1} [4,12]). Therefore, the state of stress was expected to be compressive in nature [4] for the HAPC/SS sample as was also confirmed by the experimental data obtained by the nanoindentation technique.

Table 3
Projected area (A_p) and the corresponding nanohardness (H) of the MIPS-HAP coatings.

	A_p (10^5 nm^2)	H (GPa)
Free standing HAP coating	8.40175	4.31
HAPC/SS	8.22443	4.96
HAPC/TA	8.41180	3.77

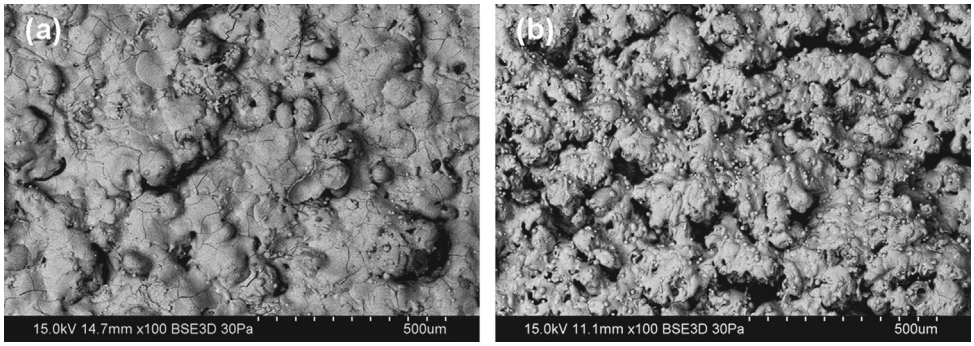

Fig. 2. E-SEM photomicrographs of the as-sprayed MIPS-HAP coatings on (a) SS316L and (b) Ti–6Al–4V substrates.

Similarly, the α value of HAP was much smaller than the α value of Ti–6Al–4V (e.g., $\alpha_{TA}=9\times10^{-6}\ K^{-1}$ [12]) alloy. Therefore, the state of stress was expected to be tensile in nature for HAPC/TA sample as was also confirmed by the experimental data obtained by the nanoindentation technique employed in the present work. These observations matched with those reported by several others other researchers [9,10,13,15].

In addition, just to adjudge the efficacy of the present nanoindentation technique, the residual stresses in the present MIPS-HAP coatings on Ti–6Al–4V and SS316L substrates, were also evaluated by the typical conventional XRD method. The following equation [26]: $\sigma_r = E_0\varepsilon$ was used for that purpose. In this Equation, σ_r is the residual stress of the coating; E_0 is the Young's modulus of the stress free virgin material e.g., the free standing coating and ε is the strain. The value of E_0 was 30 GPa. It was measured by the nanoindentation technique applied to a free standing coating. Similarly, the strain (ε) values were calculated as $[(d_c-d_0)/d_0]$ where (d_c) is the inter-planner spacing of the coating and (d_0) is the inter-planner spacing of the powder. The residual stress was evaluated as ~11 MPa for MIPS-HAP coatings on SS316L substrates and it turned out to be compressive in nature. Similarly, the present MIPS-HAP coatings on Ti–6Al–4V substrates showed a residual stress of ~12 MPa. In this case, however, the stress state was proven conclusively to be tensile in nature.

Further, the most satisfying aspect of this whole exercise was to note that, the residual stress data obtained already in the present work with the nanoindentation technique matched reasonably well with these new residual stress data obtained by the XRD based technique. In addition, it could be quite conclusively proven in the process that the matches were acceptable both in terms of the respective magnitudes of the data and the natures of the residual stress states.

4. Conclusions

Novel nanoindentation experiments showed a residual compressive stress of ~22 MPa for the MIPS-HAP coatings on the SS316L substrates. However, for the MIPS-HAP coatings deposited on the Ti–6Al–4V substrates, a residual tensile stress of ~11 MPa was estimated. These data matched well with those obtained by the more conventional XRD based technique as well as with those reported by other researchers. Thus, these facts illustrate further the efficacy of the nanoindentation based technique utilized in the present work for residual stress estimations.

Acknowledgments

AKM acknowledges the continuous encouragements of Director, CGCRI and financial supports of CSIR (Project no. NWP 0027).

References

[1] A. Dey, A.K. Mukhopadhyay, S. Gangadharan, M.K. Sinha, D. Basu, N.R. Bandyopadhyay, Nanoindentation study of microplasma sprayed hydroxyapatite coating, Ceramics International 35 (2009) 2295–2304.

[2] A. Dey, A.K. Mukhopadhyay, S. Gangadharan, M.K. Sinha, D. Basu, Development of hydroxyapatite coating by microplasma spraying, Materials and Manufacturing Processes 24 (2009) 1321–1330.

[3] A. Dey, A.K. Mukhopadhyay, S. Gangadharan, M.K. Sinha, D. Basu, Weibull modulus of nano-hardness and elastic modulus of hydroxyapatite coating, Journal of Materials Science 44 (2009) 4911–4918.

[4] A. Dey, A.K. Mukhopadhyay, S. Gangadharan, M.K. Sinha, D. Basu, Characterization of microplasma sprayed hydroxyapatite coating, Journal of Thermal Spray Technology 18 (2009) 578–592.

[5] A. Dey, A.K. Mukhopadhyay, Anisotropy in nano-hardness of microplasma sprayed hydroxyapatite coating, Advances in Applied Ceramics 109 (2010) 346–354.

[6] A. Dey, A.K. Mukhopadhyay, Fracture toughness of microplasma sprayed hydroxyapatite coating by nanoindentation, International Journal of Applied Ceramic Technology 8 (2011) 572–590.

[7] A. Dey, S.K. Nandi, B. Kundu, C. Kumar, P. Mukherjee, S. Roy, A.K. Mukhopadhyay, M.K. Sinha, D. Basu, Evaluation of hydroxya patite and β-tri calcium phosphate microplasma spray coated pin intramedullarly for bone repair in a rabbit model, Ceramics International 8 (2011) 1377–1391.

[8] J. Matejicek, S. Sampath, Intrinsic residual stresses in single splats produced by thermal spray processes, Acta Materialia 49 (2001) 1993–1999.

[9] S.R. Brown, I.G. Turner, H. Reiter, Residual stress measurements in thermal sprayed hydroxyapatite coatings, Journal of Materials Science: Materials and Medicine 5 (1994) 756–759.

[10] V. Sergo, O. Sbaizero, D.R. Clarke, Mechanical and chemical consequences of the residual stresses in plasma sprayed hydroxyapatite coatings, Biomaterials 18 (1997) 477–482.

[11] Y.C. Tsui, C. Doyle, T.W. Clyne, Plasma sprayed hydroxyapatite coatings on titanium substrates part 1: mechanical properties and residual stress levels, Biomaterials 19 (1998) 2015–2029.

[12] Y.C. Yang, E. Chang, B.H. Hwang, S.Y. Lee, Biaxial residual stress states of plasma-sprayed hydroxyapatite coatings on titanium alloy substrate, Biomaterials 21 (2000) 1327–1337.

[13] Y. Han, K. Xu, J. Lu, Dissolution response of hydroxyapatite coatings to residual stresses, Journal of Biomedical Materials Research 55 (2001) 596–602.

[14] Y.C. Yang, E. Chang, Influence of residual stress on bonding strength and fracture of plasma-sprayed hydroxyapatite coatings on Ti–6Al–4V substrate, Biomaterials 22 (2001) 1827–1836.

[15] H.C. Gledhill, I.G. Turner, C. Doyle, In vitro dissolution behaviour of two morphologically different thermally sprayed hydroxyapatite coatings, Biomaterials 22 (2001) 695–700.

[16] P. Millet, E. Girardin, C. Braham, A. Lodini, Stress influence on interface in plasma-sprayed hydroxyapatite coatings on titanium alloy, Journal of Biomedical Materials Research 60 (2002) 679–684.

[17] Y.C. Yang, E. Chang, The bonding of plasma-sprayed hydroxyapatite coatings to titanium: effect of processing, porosity and residual stress, Thin Solid Films 444 (2003) 260–275.

[18] Y.C. Yang, E. Chang, Measurements of residual stresses in plasma-sprayed hydroxyapatite coatings on titanium alloy, Surface and Coatings Technology 190 (2005) 122–131.

[19] K. Cheng, S. Zhang, W. Weng, K.A. Khor, S. Miao, Y. Wang, The adhesion strength and residual stress of colloidal-sol gel derived β-tricalcium–phosphate/fluoridated-hydroxyapatite coatings, Thin solid films 516 (2008) 3251–3255.

[20] S. Suresh, A.E. Giannakopoulos, A new method for estimating residual stresses by instrumented sharp indentation, Acta Materialia 46 (1998) 5755–5767.

[21] K.D. Bouzakis, G. Skordaris, J. Mirisidis, S. Hadjiyiannis, J. Anastopoulos, N. Michailidis, G. Erkens, R. Cremer, Determination of coating residual stress alterations demonstrated in the case of annealed films and based on a fem supported continuous simulation of the nanoindentation, Surface and Coatings Technology 174–175 (2003) 487–492.

[22] K.D. Bouzakis, N. Michailidis, Coating elastic–plastic properties determined by means of nanoindentations and FEM-supported evaluation algorithms, Thin Solid Films 469–470 (2004) 227–232.

[23] C.A. Taylor, M.F. Wayne, W.K.S. Chiu, Residual stress measurement in thin carbon films by Raman spectroscopy and nanoindentation, Thin Solid Films 429 (2003) 190–200.
[24] T. Chudoba, N. Schwarzer, V. Linss, F. Richter, Determination of mechanical properties of graded coatings using nanoindentation, Thin Solid Films 469-470 (2004) 239–247.
[25] E. Landi, A. Tampieri, G. Celotti, S. Sprio, Densification behaviour and mechanisms of synthetic hydroxyapatites, Journal of the European Ceramic Society 20 (2000) 2377–2387.
[26] I.C. Noyan, J.B. Cohen, Residual stress, Springer, New York, USA, 1987.
[27] M.H. Fathi, A. Hanifi, Evaluation and characterization of nanostructure hydroxyapatite powder prepared by the simple sol–gel method, Materials Letter 61 (2007) 3978–3983.
[28] Y. Han, S. Li, X. Wang, X. Chen, Synthesis and sintering of nanocrystalline hydroxyapatite powders by the citric acid sol–gel combustion method, Materials Research Bulletin 39 (2004) 25–32.
[29] A. Slosarczyk, Z. Paszkiewicz, C. Paluszkiewicz, FTIR and XRD evaluation of carbonated hydroxyapatite powders synthesized by wet methods, Journal of Molecular Structure 744−747 (2005) 657–661.
[30] C.Y. Yang, B.C. Wang, E. Chang, B.C. Wu, Evaluation and characterization of nanostructure hydroxyapatite powder prepared by the simple sol–gel method, Journal of Materials Science: Materials and Medicine 6 (1995) 258–265.
[31] K.A. Gross, C.C. Berndt, H. Herman, Amorphous phase formation in plasma sprayed hydroxyapatite coating, Journal of Biomedical Materials Research 39 (1998) 407–414.
[32] P. Fauchais, J.F. Coudert, M. Vardelle, A. Vardelle, A. Denoirjean, Diagnostics of thermal spraying plasma jets, Journal of Thermal Spray Technology 1 (1992) 117–128.
[33] K.A. Gross, C.C. Berndt, Biomedical application of apatites, Reviews in Mineralogy and Geochemistry 48 (2002) 631–672.
[34] R.B. Heimann, Thermal spraying of biomaterials, Surface and Coatings Technology 201 (2006) 2012–2019.
[35] K. de Groot, C.P.A.T. Klein, J.G.C. Wolke, J.M.A. de Blieck-Hogervorst, Plasma-sprayed coatings of calcium phosphate, in: T. Yamamuro, L.L. Hench, J. Wilson (Eds.), CRC Handbook of Bioactive Ceramics, CRC Press, MA, USA, 1990, pp. 3–16.
[36] A. Costan, A. Dima, I. Ionita, N. Forna, M.C. Perju, M. Agop, Thermal properties of a Ti–6Al–4V alloy used as dental implant material, Optoelectronics and Advanced Materials 5 (2011) 92–95.